Dynamics of a faceted nematic–smectic-*B* front in thin-sample directional solidification

T. Börzsönyi,[1,2] S. Akamatsu,[1] and G. Faivre[1]

[1]*Groupe de Physique des Solides, CNRS UMR 75-88, Universités Denis Diderot and Pierre et Marie Curie, Tour 23, 2 place Jussieu, 75251 Paris Cedex 05, France*

[2]*Research Institute for Solid State Physics and Optics, Hungarian Academy of Sciences, H-1525 Budapest, P.O. Box 49, Hungary*

(Received 5 June 2001; published 13 December 2001)

We present an experimental study of the directional-solidification patterns of a nematic–smectic-*B* front. The chosen system is $C_4H_9-(C_6H_{10})_2CN$ (in short, CCH4) in 12 μm-thick samples, and in the planar configuration (director parallel to the plane of the sample). The nematic–smectic-*B* interface presents a facet in one direction—the direction parallel to the smectic layers—and is otherwise rough and devoid of forbidden directions. We measure the Mullins-Sekerka instability threshold and establish the morphology diagram of the system as a function of the solidification rate V and the angle θ_0 between the facet and the isotherms. We focus on the phenomena occurring immediately above the instability threshold when θ_0 is neither very small nor close to 90°. Under these conditions, we observe drifting shallow cells and a type of solitary wave, called ''faceton,'' which consists essentially of an isolated macroscopic facet traveling laterally at such a velocity that its growth rate with respect to the liquid is small. Facetons may propagate either in a stationary or an oscillatory way. The detailed study of their dynamics casts light on the microscopic growth mechanisms of the facets in this system.

DOI: 10.1103/PhysRevE.65.011702 PACS number(s): 64.70.Md, 81.10.Aj, 64.70.Dv, 68.70.+w

I. INTRODUCTION

A crystal growing from an undercooled melt rejects heat and chemical species, which must diffuse away in the liquid for the process to continue. The thus-generated thermal and solutal gradients tend to destabilize the advancing solid-liquid interface. This effect is counterbalanced by the surface tension and the so-called interfacial kinetics, which tends to slow down the progression of the interface, and hence, stabilize it. As a result of the competition between these conflicting factors, solidification fronts may assume a large variety of nonlinear patterns, the characteristics of which depend on the control parameters, and the initial and boundary conditions of the process.

The study of solidification patterns has been an active field of research for several decades [1–3]. Most of the existing studies are devoted to fully nonfaceted systems. In such systems, the surface tension γ and the kinetic coefficient β (defined as the ratio of the kinetic undercooling to the growth velocity) are nonsingular functions of the orientation of the interface with respect to the crystal lattice. On a molecular scale, this corresponds to the fact that the interface is rough in all orientations. Familiar aspects of the dynamics of fully nonfaceted systems in directional solidification, i.e., when the system is pulled at a constant velocity V toward the cold side of an applied unidirectional thermal gradient G (see Fig. 1), are the existence of a stable planar front at low values of V, the primary cellular (or Mullins-Sekerka) instability occurring at a threshold velocity V_c, the quasiperiodic arrays of rounded cells at V slightly above V_c, and of dendrites at V much higher than V_c. Many dynamical features of these patterns (e.g., stability limits, modes of instability) are not yet fully understood, but some of their fundamental properties are now clear, among which the crucial role played by interfacial anisotropy [1,4,5]. In fact, a certain minimum degree of interfacial anisotropy is a necessary condition for cellular and dendritic arrays to be stable, or even to exist. In thin samples—i.e., quasibidimensional (2D) systems—γ and β are functions of a single variable, say, the tilt angle θ of the interface with respect to the isotherms. The functions $\gamma(\theta)$ and $\beta(\theta)$, and thus the solidification patterns, depend on the orientation of the crystal with respect to the solidification setup [6–8].

In contrast with the case of fully nonfaceted systems, little is yet known about the directional-solidification dynamics of faceted crystals. The few existing experimental studies on this subject first of all show that a distinction must be made between fully and partly faceted systems [6,9–12]. Growth facets (which most generally, although not necessarily, coincide with equilibrium facets [13]) correspond to planes of the crystal containing several directions of strong binding. Fully faceted crystals have numerous facet directions, and their directional-solidification fronts consist of a succession of facets limited by sharp edges. The dynamics of such fronts does not give rise to any stationary state, in general, and bears no obvious relation with that of nonfaceted fronts. Partly faceted systems only have a few facet directions connected to one another by large rounded regions. In lamellar crystals, the solid-liquid interface may be rough in all but one direction, namely, that of the molecular layers. In this case, when the tilt angle θ_0 of the layers with respect to the

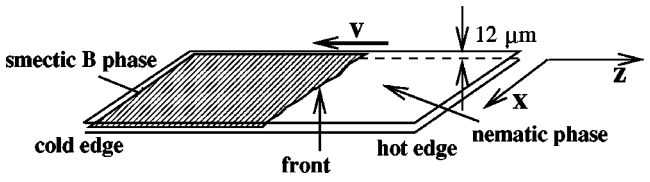

FIG. 1. Sketch of a thin-sample directional-solidification setup. *z*: axis of the thermal gradient; *x*: axis parallel to the isotherms; *V*: pulling velocity. After a transient, the front advances (in average) at the imposed velocity *V* with respect to the liquid, and thus remains essentially immobile in the laboratory reference frame. It can then be continuously observed with an optical microscope.

isotherms is large, the dynamics of the front must obviously be that of a nonfaceted crystal as long as the deformation of the front remains small, that is, below V_c and in a small range of V above V_c. Facets only appear at higher V when the deformation of the interface is large. A relatively smooth transition from the nonfaceted to partly faceted dynamics may then be observed. This is the experimental configuration considered in this study.

In this paper, we study the directional-solidification dynamics of the front associated to the nematic–smectic-B transition of the liquid-crystal $C_4H_9-(C_6H_{10})_2CN$ (in short, CCH4). A long-range order exists in the direction perpendicular to the molecular layers in the smectic-B phase, so that this phase actually is a lamellar crystal. Previous free-growth studies have indeed shown that the nematic–smectic-B fronts of the $n=3,4,5$ members of the series CCHn (where n stands for the number of carbon atoms in the aliphatic chain) have a single facet direction parallel to the molecular layers of the smectic phase, and are rough in all other directions [14–16]. Moreover, they have no unstable orientations in a direction perpendicular to the molecular layers, contrary to the smectic-A–smectic-B fronts previously studied in directional solidification by Melo and Oswald and Oswald *et al.* [6,11,12]. The present study is performed in thin (12 μm-thick) samples and in the planar configuration (director parallel to the plane of the sample), in order for the front—including the facets, if any—to remain perpendicular to the sample plane. Practically, the system is thus a 2D one.

We shall mostly focus on a type of solitary wave appearing near the Mullins-Sekerka threshold, called ''faceton'' because it contains a single small facet traveling along the front at such a velocity that the normal growth rate of the facet, i.e., its growth rate with respect to the liquid, is generally much smaller than V. Such a phenomenon, which has never been observed before, to the best of our knowledge, is obviously highly specific to faceted directional solidification, and therefore particularly interesting from our present viewpoint. A preliminary comment about the nematic–smectic-B facets in the CCHn series is in order. The growth rate of a facet is controlled by the dynamics of the molecular steps flowing along it. Therefore, it crucially depends on whether or not the facet contains, or is connected with, step sources [13,17]. When no step source is available, the facet grows through nucleation and spreading of terraces (surface nucleation), which is a very slow process at low undercooling. In fact, the growth rate of a perfect facet is totally negligible when the undercooling is lower than some finite value. Such a behavior (''blocked'' facets at low undercoolings) has clearly been observed during the solidification of many, but not all the studied faceted systems. What concerns us here is that it was not observed during the free growth of the smectic-B phase of CCH3, despite the strongly faceted aspect of the growing crystals [14–16]. Numerical simulations in which a cusplike minimum of $\gamma(\theta)$ but no anisotropy of β was taken into account satisfactorily reproduced the observed growth shapes. Thus, the observation of a facet on a macroscopic scale would not necessarily mean the presence of a singularity in β. In order to clarify this point in the case of CCH4, we report, in Sec. III, preliminary observations in free growth showing that the nematic–smectic-B facet of CCH4 is capable of remaining immobile at undercoolings lower than 0.1 K. Thus, in CCH4 at least, the nematic–smectic-B fronts can form growth facets.

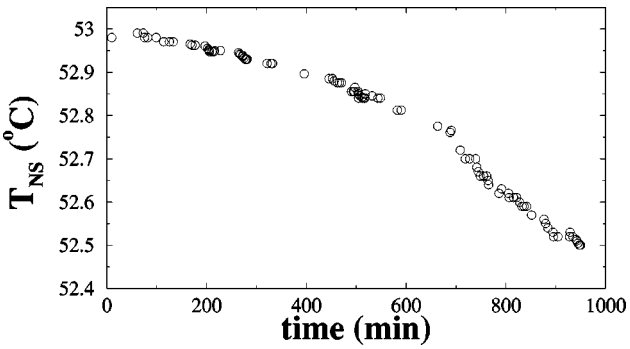

FIG. 2. The nematic–smectic-B equilibrium temperature in a CCH4 sample as a function of time. T_{NS} was measured by controlling the temperature of a free-growth stage in order to keep a small smectic-B crystal in quasiequilibrium with the nematic. The relatively low initial value of T_{NS} indicates that the sample was rather impure at the outset.

II. EXPERIMENT

The relevant material parameters of the liquid-crystal CCH4 (MERCK IS-0558) may be found in Ref. [15]. The residual impurities, the chemical nature of which is unknown, were characterized as regards solidification by the usual methods (see below). We found that the impurity content at the outset of the experiments was reproducible, but slowly increased during the experiments, indicating that the product was undergoing a decomposition in the nematic phase, as previously noticed and analyzed for the case of CCH3 [18]. The nematic–smectic-B transition temperature T_{NS} was generally of about 53.1 K in fresh samples. Figure 2 shows T_{NS} measured as a function of time in one sample. It can be seen that the decomposition rate is sufficiently slow not to severely perturb a solidification run, but sufficiently rapid to prevent us to carry out several successive runs with the same sample. Outgasing the as-received product resulted in a significant slowing down of the decomposition process.

We have studied the crystal structure of the smectic-B phase of CCH4 by low-angle x-ray diffraction [19]. As expected, this phase is basically an AB-type stacking of hexagonal layers. The parameters are approximately $a=5.9$ Å and $c=29$ Å, which is in accordance with the data available for the other members of the homologue series [20]. The hexagonal layers however appear to be slightly distorted, which may entail the existence of superstructures in the layers.

A schematic view of a thin-sample directional-solidification experiment is shown in Fig. 1. A detailed description of our setup is given elsewhere [7,8]. In this study, the samples were made of two parallel glass plates separated by 12-μm-thick plastic spacers. Their useful width was of 9 mm and their length of 60 mm. They were filled under an argon atmosphere at a temperature higher than T_{NS}, and then

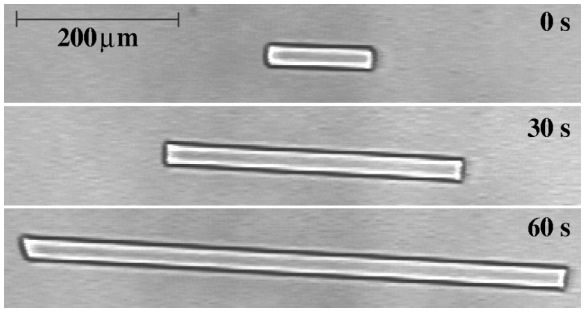

FIG. 3. Free growth. Successive snapshots of a smectic-*B* crystal of CCH4 growing from the nematic phase at $\Delta T = 0.07$ K.

cooled down to room temperature. Numerous smectic crystals appeared by heterogeneous nucleation during cooling. The samples were placed in the thermal gradient, and a smectic-*B* crystal of known orientation (determined through the observed value of θ_0) was selected by a method to be explained shortly. The sample was annealed at rest for about 30 minutes in order to homogenize the concentration in the liquid. V was then switched to a chosen value, left for a given time at this value, and then increased step by step. The temperature gradient at the growth front was of 53 $\mathrm{K\,cm^{-1}}$, unless otherwise mentioned. The pulling velocity was in the range of 0.3–30 $\mu\mathrm{m\,s^{-1}}$. The observations were made with a polarizing microscope (Leica) equipped with a charge-coupled device camera. The video signal was analyzed with digital image processing.

It is obviously crucial for our experiments that large smectic-*B* crystals of arbitrary orientation might be selected. To this aim, we have studied the influence of various treatments of the inner sides of the glass plates. Three types of plates were used: untreated plates, plates covered with a monooriented thin film of poly(tetrafluorethylene) prepared by friction transfer at $T \approx 200\,^{\circ}\mathrm{C}$ [21], or with a ≈ 100 Å-thick layer of Al or In deposited by oblique evaporation. In the nematic phase, the orientation of the director was essentially planar in all samples. The director was more or less aligned along the direction of friction, or deposition, in treated samples, but domains corresponding to small (a few degrees) variations in the orientation of the director, still existed (see Fig. 4 below). This inhomogeneity of the nematic phase caused but minor perturbations in our experiments, since the phenomena of interest turned out to be essentially independent of the orientation of the nematic director. In all samples, the smectic-*B* phase had a planar orientation, but was divided into different crystals (or grains) corresponding to a different value of θ_0. The surface treatment gave a pronounced preferential distribution of θ_0 among the various grains, facilitating the selection of the desired value of θ_0. The size of the selected smectic-*B* grain was increased by a method consisting of forcing the crystal to grow through a funnel-shaped obstacle [7]. By this method, smectic grains of a millimetric width, and arbitrary values of θ_0 were obtained.

III. CHARACTERIZATION OF THE SYSTEM

A. Free growth at small undercoolings

The observations reported in this section were performed with a free-growth setup similar to the one described in Ref.

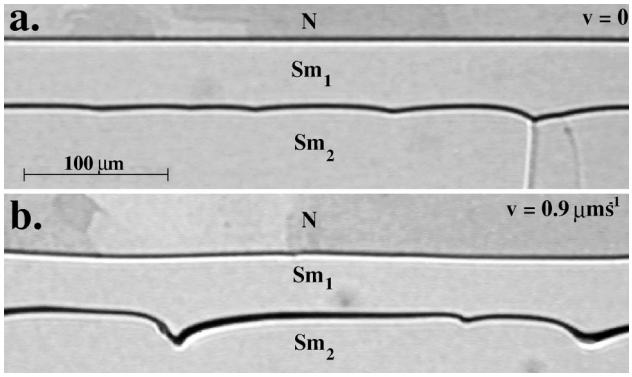

FIG. 4. Directional solidification (in this, and all the following micrographs, growth is upwards). N: nematic; Sm1: smectic-*B*; Sm2: smectic-*B* oriented differently from Sm1. (a) Sample at rest ($V=0$); (b) sample in the process of solidification at $V = 0.9\ \mu\mathrm{m\,s^{-1}}$. Note the domains in the nematic. Sm1 is a single crystal, but Sm2 is a polycrystal, as shown by the presence of cusps on the Sm1-Sm2 front.

[22], in which the changes in the undercooling are produced, via the Clausius-Clapeyron effect, by a sudden pressure change at constant temperature, and are therefore quasi-instantaneous [22,23]. The samples were the same as those used in directional solidification. At the beginning of the experiments, the samples were heated step by step until only one small smectic-*B* crystal was left in the nematic. The sample was maintained at constant temperature until the changes in the shape of the crystal became very slow (this took about 20 minutes). Admittedly, this shape is not the exact equilibrium shape of the crystal, but it exhibits clear reproducible features, namely, long facets parallel to the smectic layers and rounded ends in the perpendicular direction [Fig. 3 (a)], which is enough for our present purpose. It should be noted that the observed near-equilibrium shape clearly shows the absence of a forbidden orientation range around $\delta\theta = 90°$, where $\delta\theta$ is the deviation of the interface from the direction of the molecular layers, but suggests that the facet might actually be limited by a sharp edge, i.e., the interface might be unstable at small values of $\delta\theta$. The fact that we have not observed the Herring instability [24,11] in directional solidification at the lowest-explored value of θ_0 indicates that this forbidden orientation range is very small ($<2°$), if it exists at all.

A sudden increase of the undercooling δT was applied at time $t=0$, and the subsequent growth of the crystal recorded (Fig. 3). The growth process, which is governed by the anisotropic interfacial properties and diffusivities, is very complicated. Its study is beyond the scope of this paper. Here, we limit ourselves to the following observation: the facets of the smectic-*B* crystals remained blocked within experimental uncertainty (their growth rate was lower than about 0.01 $\mu\mathrm{m\,s^{-1}}$) at undercoolings lower than 0.1 K (Fig. 3). At higher undercoolings, they generally grow at a measurable rate. The apparent threshold undercooling ΔT_{nucl} for growth by surface nucleation of our system is thus larger than 0.1 K and probably not much larger than this value. This estimate of ΔT_{nucl} is small compared to what it is in ordinary solid-

liquid systems, but this may be explained by the small value of γ in our system [25,26]. It is also possible that in our thin samples, surface nucleation is in fact heterogeneous, i.e., takes place preferentially along the line of contact with the glass plates. The nucleation rate would then depend on the treatment of the glass plates.

B. Directional solidification: Instability threshold

The Mullins-Sekerka instability threshold was found to lie between approximately 2 and $3\,\mu\mathrm{m\,s^{-1}}$ in all the studied (fresh) samples. No influence of the orientation of the smectic, or the nematic was observed within experimental uncertainty. However, it should be noted that this uncertainty was large ($\approx 1\ \mu\mathrm{m\,s^{-1}}$) for the reason to be explained presently.

Figure 4 shows a sample at rest, and pulled at a rate lower than V_c. Two isothermal fronts are visible, namely, a front separating the nematic (N) phase from a smectic-*B* domain (Sm1), and at a lower temperature, a front separating Sm1 from a second smectic-*B* domain (Sm2). The nature of the transition from Sm1 to Sm2 is not yet clear. This transition was observed in most, but not all experiments. Observations (not reported here) incline us to think that Sm2 is the same phase as Sm1, but with a different orientation, thus, a different interaction energy with the glass plates. In any case, we need not take into account the Sm1-Sm2 front here since this front, when present, does not perturb the dynamics of the N-Sm1 front.

It can be seen in Fig. 4 that the nematic–smectic-*B* front remains planar during solidification at $V<V_c$, except for small, long-wavelength distortions due to the presence of domains in the nematic phase. These distortions are larger during solidification than at rest, and undergo sudden changes each time the front leaves a nematic domain for another. This phenomenon has thus an equilibrium as well as a kinetic origin. In our experiments, it plays the role of a relatively strong, long-wavelength, low-frequency noise, which blurs some of the morphological-transition thresholds of the system. This is the main origin of the aforementioned large uncertainty on the measured values of V_c. However, we may state with certainty that V_c was higher than $2\ \mu\mathrm{m\,s^{-1}}$ since the distortions caused by nematic domains, or any other source of perturbation (e.g., dust particles) did not amplify below this velocity.

C. Solute redistribution transient

When V is smaller than V_c, the front reaches a stationary planar state through the so-called solute redistribution transient. A recoil curve—i.e., the curve representing the variation of the position (or temperature) of the planar front as a function of time during the initial transient of a particular run—is reproduced in Fig. 5. It is well known that information about the relevant properties of the solute (diffusion coefficient D in the liquid, partition coefficient K, thermal gap ΔT_o) may be gained from the characteristics of the transient, and the value of V_c. We have utilized this method in order to characterize the unknown impurity playing the role of solute in our system.

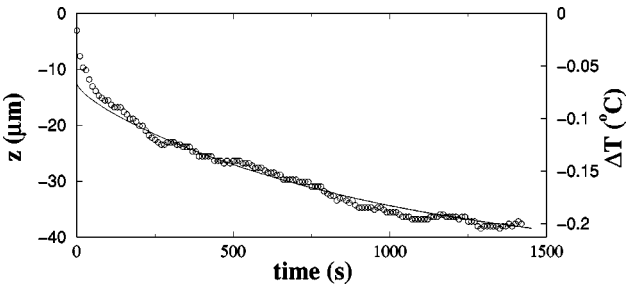

FIG. 5. Recoil curve at $V=0.9\ \mu\mathrm{m\,s^{-1}}$. Same run as in Fig. 4. Continuous line: best fit according to the Warren-Langer approximation. The rapid decrease at the onset of the recoil is an instrumental effect.

The threshold velocity, and the amplitude of the solute redistribution transient are given by $V_c \approx (1+KD^s/D)DG/\Delta T_o$ (D^s: diffusion coefficient in the solid) and ΔT_o, respectively, [27]. By fitting the recoil data using the Warren-Langer approximate theory [28] (Fig. 5) and assuming $V_c = 2.5\ \mu\mathrm{m\,s^{-1}}$ and $KD^s/D \ll 1$, we obtained $K=0.12$. This gives $D=80\ \mu\mathrm{m^2\,s^{-1}}$ and $\Delta T_o = 0.2$ K. These data give us no information about D^s, but there is good reason to believe that our system is a two-sided one—i.e., that D^s is not much smaller than D [12].

IV. RESULTS

A. Morphology diagram

A diagram displaying the observed morphologies as a function of the pulling velocity and the orientation of the smectic-*B* crystal is shown in Fig. 6.

It can be seen that the sequence of morphologies observed as a function of V for a fixed value of θ_0 is the same for all

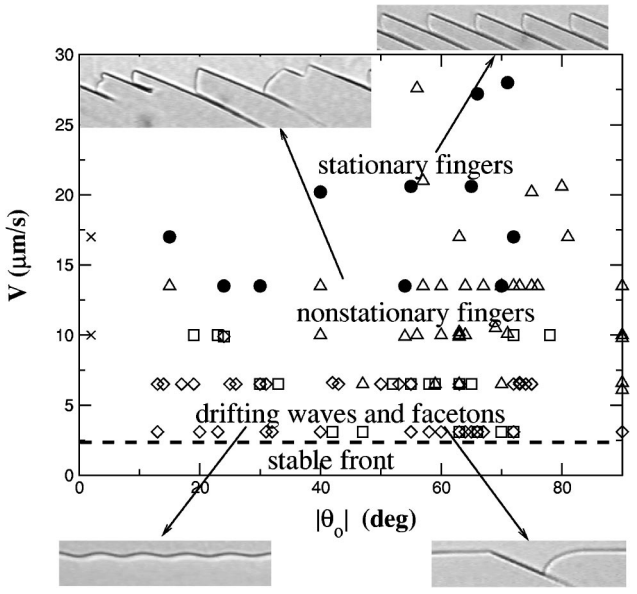

FIG. 6. Morphology diagram. Measurement points: waves and facetons (◇), facetons and unstationary faceted fingers (□), unstationary faceted fingers (△), stationary faceted fingers (●), and unstable facets (x). Heavy dashed line: Mullins-Sekerka instability threshold. Inset micrographs: see Fig. 7.

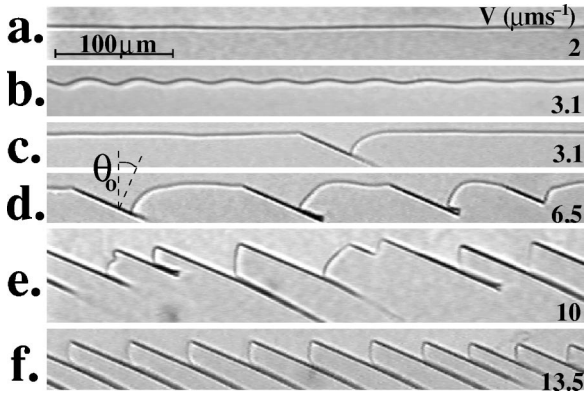

FIG. 7. The different growth morphologies observed as a function of V for $\theta_0 = 25°$. (a) Planar front; (b) drifting shallow cells; (c) drifting faceton (stationary mode); (d) drifting facetons (oscillatory mode) at different stages of their oscillation cycle; see Fig. 18 below; (e) nonstationary array of faceted fingers ; (f) stationary array of faceted fingers.

values of θ_0, except for those close to 0° (facets parallel to the growth front) or 90° (facets perpendicular to the growth front). This generic sequence is illustrated in Fig. 7.

Small-amplitude, nearly sinusoidal traveling waves appear near the instability threshold [Fig. 7(b)], in accordance with previous observations in two-sided anisotropic systems [6]. Such weakly nonlinear waves are commonly called ''shallow cells.''

We observed drifting shallow cells in a broad range of V around the threshold ($1\ \mu\mathrm{m\,s^{-1}} \leqslant V \leqslant 8\ \mu\mathrm{m\,s^{-1}}$). In the same range of V, we also observed ''facetons'' [Fig. 7(c)]. These solitary waves may propagate in a stationary or an oscillatory way. They appear when the amplitude of the cells is so large that the tilt angle of the front locally reaches the value θ_0 corresponding to the facets. Most generally, this occurs under the effect of perturbations due to the nematic domains. The frequency of creation of facetons, and thus, their average number by unit length of the front increases as V increases. When the average spacing of the facetons becomes smaller than their width ($\approx 200\ \mu\mathrm{m}$), they cease to behave as non-interacting objects. In fact, they disappear altogether, giving way to arrays of much narrower objects, called faceted fingers [Fig. 7(e)]. This occurs at about $8\ \mu\mathrm{m\,s^{-1}}$. However, this transition is strongly noise dependent, and thus, relatively ill defined from an experimental viewpoint. Shallow cells and facetons are studied in detail in the next section.

The arrays of faceted fingers, which are observed above $8\ \mu\mathrm{m\,s^{-1}}$ exhibit a relatively sharp transition from an unstationary [Figs. 7(e) and 8] to a stationary dynamics as V increases (Figs. 7(f) and 9; the dispersion appearing in Fig. 6 is mostly due to the aging of the samples). The spatiotemporal diagrams of the unstationary arrays shown in Fig. 8 reveal the transitory or local existence of well-defined oscillatory modes. These modes become more and more apparent as V increases because the oscillation period T_{osc} is a rapidly decreasing function of V [Fig. 10(a)]. This strongly suggests the existence of a homogeneous oscillatory bifurcation of the

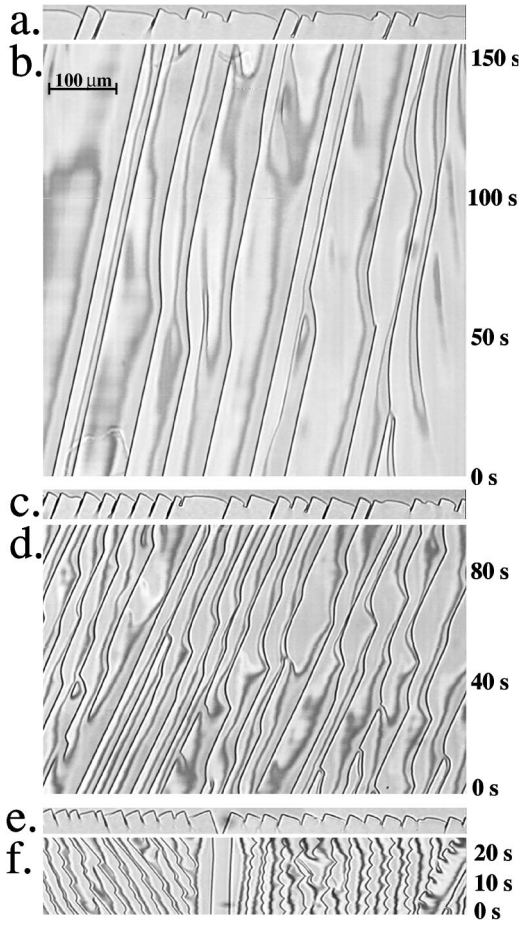

FIG. 8. Transition from isolated facetons to faceted fingers for $\theta_0 = -70°$ in an aged sample. (a) $V = 3.1\ \mu\mathrm{ms^{-1}}$ (snapshot of the front); (b) corresponding spatiotemporal diagram (time series of the intensity distribution along a line located 20 μm below the front); (c) $V = 6.5\ \mu\mathrm{m\,s^{-1}}$; (d) corresponding spatiotemporal diagram; (e) $V = 13.5\ \mu\mathrm{m\,s^{-1}}$. Note that another grain ($\theta_0 = 73°$) appears in the leftmost part of the figure; (f) corresponding spatiotemporal diagram.

high-V stationary patterns as V decreases within some narrow range of spacing.

We now turn to the particular orientations corresponding to the bounds of the scanned interval of θ_0. When $\theta_0 = 90°$, the system is reflection symmetric. Shallow cells no longer drift, and facetons cease to exist. The shallow cells break up into narrow faceted fingers as V is increased above threshold [Fig. 11(a)]. The widest faceted fingers, which are the majority ones, are not reflection symmetric, whereas the narrowest ones are reflection symmetric. The two opposite but equivalent directions of symmetry breaking are equally populated. The resulting arrays were nonstationary even at the highest-explored values of V [Fig. 11(b)]. This is very different from what was observed by Oswald *et al.* in smectic-*A*-smectic-*B* fronts for a similar orientation of the facet [6]. In that system, because of the existence of forbidden directions, the finger tips exhibited pointed triangular shapes, and formed stationary arrays.

When θ_0 is sufficiently close to zero, the growth front of smectic-*B* grains is entirely occupied by a facet at any value

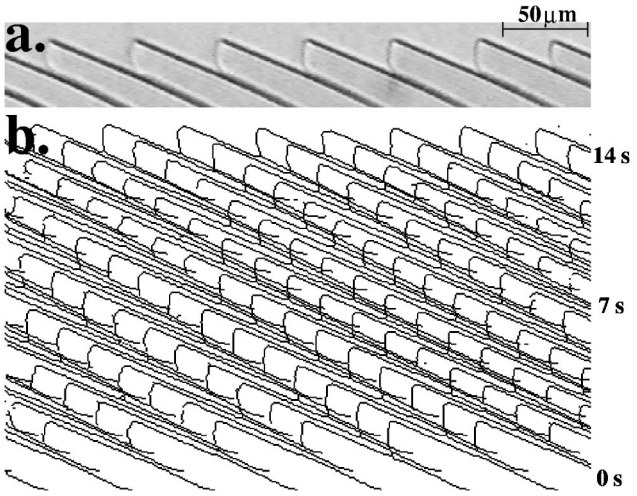

FIG. 9. Stationary array of faceted fingers at $V=13.5\ \mu\mathrm{m\,s^{-1}}$ and $\theta_0=24°$. (a) Snapshot of the front; (b) spatiotemporal diagram (piling up of skeletonized images of the growth front).

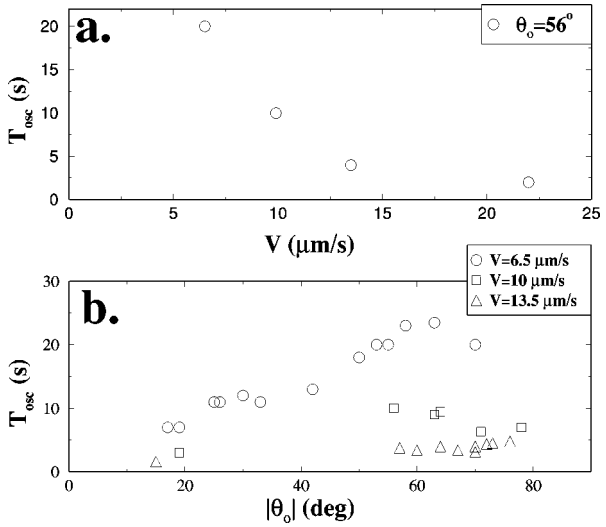

FIG. 10. Oscillation period (a) as a function of V for $\theta_0=56°$ (b) as a function of $|\theta_0|$ for three values of V. The leftmost point in (a) corresponds to an isolated oscillatory faceton.

of V. This may be considered as a finite-size effect resulting from the following fact: facets are always present in the grooves attached to grain boundaries for whatever values of θ_0 and V; the stationary size of these facets is more or less proportional to $1/(\tan|\theta_0|)$; they thus occupy the whole grain when $|\theta_0|$ is lower than a certain value, which is of about 2° for a grain size of 500 μm. At sufficiently high V, these long facets break up through the mechanism illustrated in Fig. 11(c). It is not necessary to repeat here the description of this process, which has been presented by other authors [12]. We simply note that, in our fresh samples, this instability was observed to result from the occasional collisions of the front with defects (domain walls, dust particles) present in the nematic. In the less pure samples, it was superseded by another well-known process, namely, the nucleation of crystals in the undercooled melt ahead of the front [6]. Both mechanisms give rise to more or less permanently cyclic growth regimes.

B. Near-threshold patterns

1. Drifting shallow cells

Most generally shallow cells appeared in the form of a noise-induced wave packet. A spontaneous homogeneous growth of the cells was never observed with certainty. We attribute this fact to the interplay between shallow cells and facetons (see below). At, or below 2 $\mu\mathrm{m\,s^{-1}}$, noise-induced wave packets systematically disappeared when the source of noise disappeared, as already mentioned. At higher V, they evolved as illustrated in Figs. 12 and 13.

A careful analysis of the spatiotemporal diagram of Fig. 12 has shown that (i) the cells are initially sinusoidal; (ii) they grow in amplitude with a uniform amplification rate of $\approx 0.002\ \mathrm{s^{-1}}$; (iii) the amplest cells are no longer sinusoidal at the end of the time sequence, (iv) the spacing λ and the drift velocity V_d are uniform in space and constant in time. V_d is thus amplitude independent. This is in keeping with the idea that this sequence is the initial stage of the usual amplification process leading from a linearly unstable state to a stationary weakly nonlinear regime. The final regime was not observed because the process was interrupted by an external perturbation giving rise to a faceton.

The traces on the lefthand side of Fig. 13 are the trajectories of three oscillatory facetons. These objects are studied below. For now, the point of interest is that the rearmost faceton leaves behind a region of the front that is free of detectable shallow cells (see also Figs. 15 and 18 below). The cells reappear at ≈ 200 μm from the faceton, and then amplify following a process entirely similar to the above

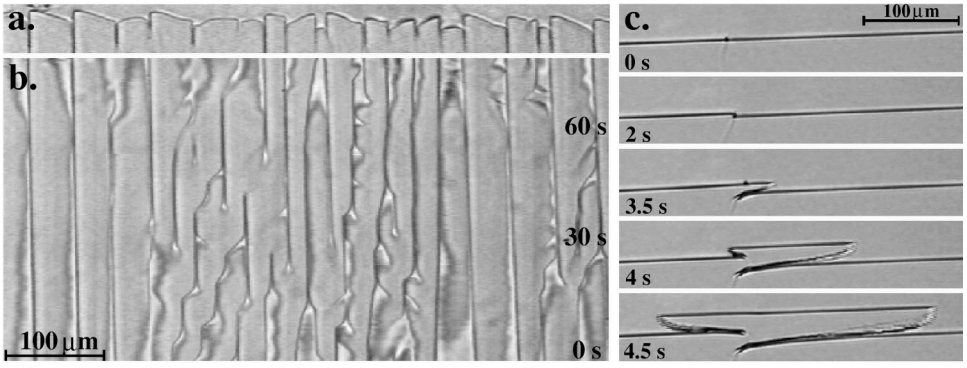

FIG. 11. (a) Array of symmetry-broken faceted fingers at $\theta_0=90°$ and $V=10\ \mu\mathrm{m\,s^{-1}}$; (b) corresponding spatiotemporal diagram; (c) instability of a facet at $\theta_0=2°$ and $V=10\ \mu\mathrm{m\,s^{-1}}$.

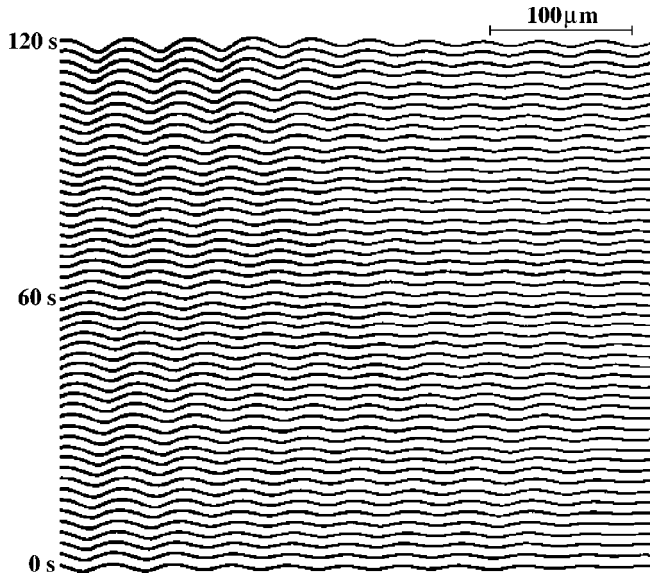

FIG. 12. Spatiotemporal diagram of a drifting wave packet; $V=3.1\ \mu\mathrm{m\,s^{-1}}$, $\theta_0=25°$.

one, except for two points: (i) in the present case, the amplification rate ($\approx 0.02\ \mathrm{s^{-1}}$) is much larger than in the preceding case, since V is higher, and (ii) a stationary regime of nonlinear shallow cells is reached. This confirms clearly, although only semiquantitatively, that the system admits stationary weakly nonlinear cellular states within a measurable range of V above V_c. These states are metastable with respect to the formation of facetons. Also, we note that the direction of drift of the cells is opposite to that of facetons. This is somewhat of a surprise since, in other systems, shallow cells and facets have been found to drift in the same direction [6].

The measured values of $|V_d|$ and λ are plotted in Fig. 14 as a function of θ_0 for a given value of V. The data are compatible with the fact that $V_d(\theta_0)$ must go to zero at $\theta_0=0°$ and 90° for symmetry reasons. The maximum is at about 70°, and corresponds to a relatively large value of V_d/V, indicating that the system is strongly anisotropic even in the orientation range in which the interface is rough.

We have noted above that V_d seems to be independent of the amplitude of the cells. It is thus legitimate to admit (but not certain) that the measured value of V_d is the same as in the linear regime. We have performed a linear stability analysis of the planar front of a two-sided system taking into account the anisotropy of the diffusion in the two bulk phases (nematic and smectic-*B*), and that of the linear kinetic coefficient β (the anisotropy of γ does not come into play in a linear calculation [4]). We have solved the dispersion equation numerically under various assumptions concerning the orientation dependences of D, D_s, and β, which are not known. Qualitatively, the results may be summed up as follows [27]. We find that the observed sign and absolute value of $V_d(\theta_0)$ could be ascribed to diffusion anisotropy only if, in the smectic-*B* phase, the impurities diffused much faster through the smectic layers than parallel to them, which is very unlikely to be true. Thus, the observed drift of the shallow cells is most probably due to kinetic anisotropy. In such a case, the sign of V_d is given by $-d\beta/d\theta$ [4]. In conclusion, the observed direction of drift of the shallow cells (if it is really the same as in the linear regime) indicates that, in our system, β increases as $\delta\theta$ increases. This result poses no particular problem except for the vicinal domain, in which β is expected to be more or less proportional to the reciprocal of the step density, and hence, to the reciprocal of $\delta\theta$ [29]. The crossover from the vicinal to the rough domains as $\delta\theta$ increases should thus manifest itself through a change in the sign of V_d. It is tempting to assume that this crossover cor-

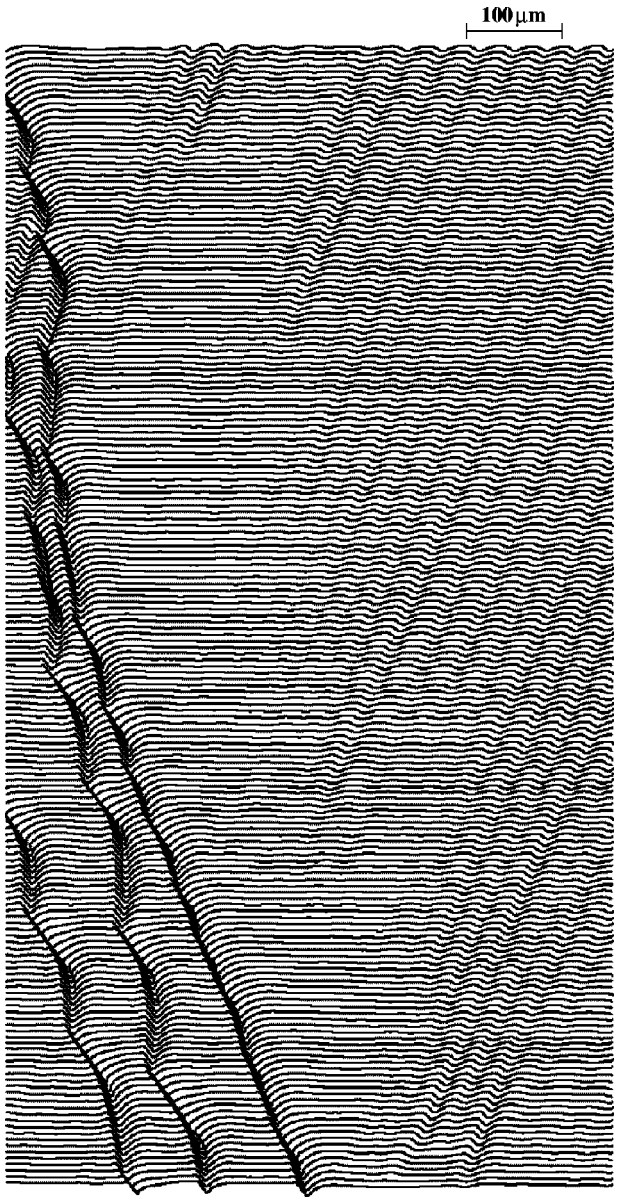

FIG. 13. Spatiotemporal diagram. The three traces on the left-hand side are the trajectories of oscillatory facetons drifting leftwards. Note the disappearance of the cells (which drift rightwards) in the wake of the rearmost faceton. A temporary exception to this rule is visible near the end of the recording, when the faceton emits a packet of three or four cells. This exception is only apparent, however, since this occurs during a period of time when the faceton no longer exists (it is drifting rightwards). $V=6.5\ \mu\mathrm{m\,s^{-1}}$, $\theta_0=55°$, recording time $=250$ s.

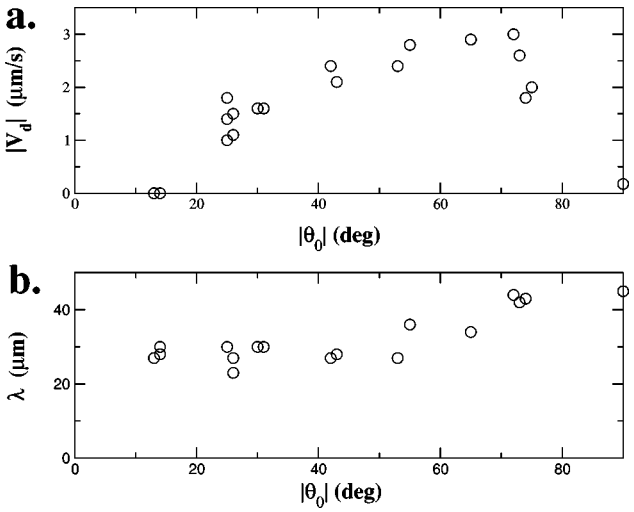

FIG. 14. Drift velocity (a) and wavelength (b) of the cells as a function of the tilt angle of the facet at $V=6.5\ \mu\mathrm{m\,s^{-1}}$.

responds to the zero of $V_d(\theta_0)$, which perhaps appears near 12° in Fig. 14(a). However, the observation of macroscopic facets drifting in the same direction as the shallow cells disproves this assumption, and indicates that the vicinal domain is actually very narrow in our system (see below).

2. Stationary facetons

The spatiotemporal diagram of a stationary faceton is shown in Fig. 15. Clearly, a faceton is a solitary wave consisting of a macroscopic facet and a broad rounded finger separated from each other by a very thin liquid groove. The regularity of the spatiotemporal diagram shows that facetons, once formed, are quite stable. In particular, they absorb the shallow cells that they may encounter ahead of themselves without being modified, and seem to be insensitive to the perturbations caused by the nematic domains. The depth of the facet—i.e., the distance Δz_f between the two edges of the facet along the z axis—is difficult to measure with accuracy because the lower edge, located near the bottom of the groove, is generally not resolved. However, it is certain that Δz_f is in the $30-50\ \mu$m range (the difference of temperature ΔT_f between the two edges is thus in the range 0.15–

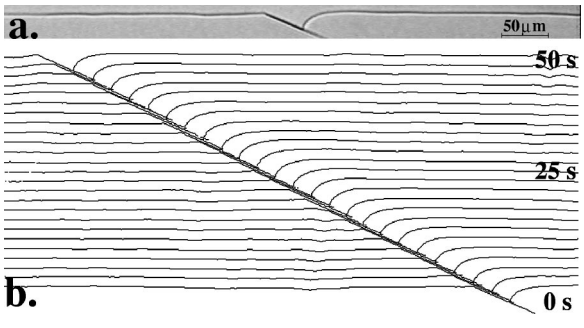

FIG. 15. Stationary faceton. $\theta_0=25°$, $V=6.5\ \mu\mathrm{m\,s^{-1}}$. (a) Snapshot of the front. The faint dark line appearing in the solid in the continuation of the facet is a thin liquid groove; see Fig. 17. (b) Spatiotemporal diagram. The normal growth rate of the facet is $V_n \approx 0.9\ \mu\mathrm{m\,s^{-1}}$.

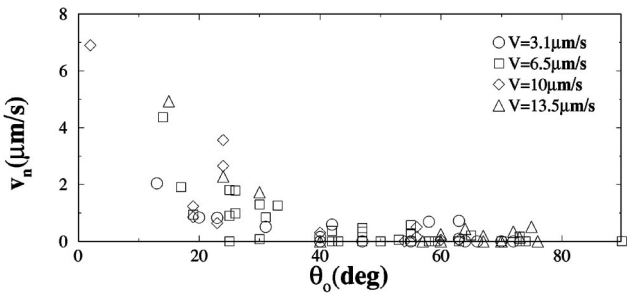

FIG. 16. Normal growth velocity of facets belonging to facetons or arrays of faceted fingers as a function of the tilt angle of the facet for the indicated values of the pulling velocity. In the case of oscillatory facetons, the minimum value of V_n has been plotted. The data point at $\theta_0=2°$ corresponds to the facet shown in Fig. 11(c) prior to its destabilization.

0.25 K), and decreases as θ_0 increases. The upper edge of the facet corresponds to a small pointed maximum of the front shape, but it is not possible to decide whether, or not, this edge is sharp on a molecular scale. The width of the rounded finger—i.e., the extension of the deformed region of the front behind the finger tip—is of about 200 μm. As mentioned, shallow cells do not develop in this region of the front. The trajectory of the faceton makes a small angle with the direction of the macroscopic facet, indicating that the normal growth rate of the facet is small but finite. Thus, the facet is not blocked, and the question arises as to its microscopic growth mechanisms.

Figure 16 displays a large number of values of the normal velocity of facets V_n measured in isolated facetons as well as in arrays of faceted fingers for various values of V and θ_0. In spite of a large dispersion of the data, it is clear that V_n is essentially a nonzero quantity that decreases as θ_0 increases, and increases as V increases. The regularity of the stationary facetons or arrays (see Figs. 15 and 9), and the fact that V_n is very close to zero when θ_0 is large allow us to exclude screw dislocation growth as the dominant mechanism. Moreover, the fact that both V_n and Δz_f are decreasing functions of θ_0 suggests that V_n is essentially determined by events occurring near the lower edge of the facet. One may imagine either that surface nucleation takes place at a relatively high rate at this point, or that the facet is supplied with steps coming from the bottom of the groove where the interface is necessarily rough. In both cases, V_n would be very sensitive to the details of the conformation of the interface in this region. These details may depend on the treatment of the glass plates, which could explain the dispersion between values measured in different samples.

3. Oscillating facetons

Figure 17 shows a process of formation of facetons in response to a perturbation. Macroscopic facets progressively develop on one side of the shallow cells as the amplitude of the latter increases. These facets first drift with the same velocity as the shallow cells, and then change their direction of drift. This change is not accompanied by any modification in the orientation of the facets within experimental uncer-

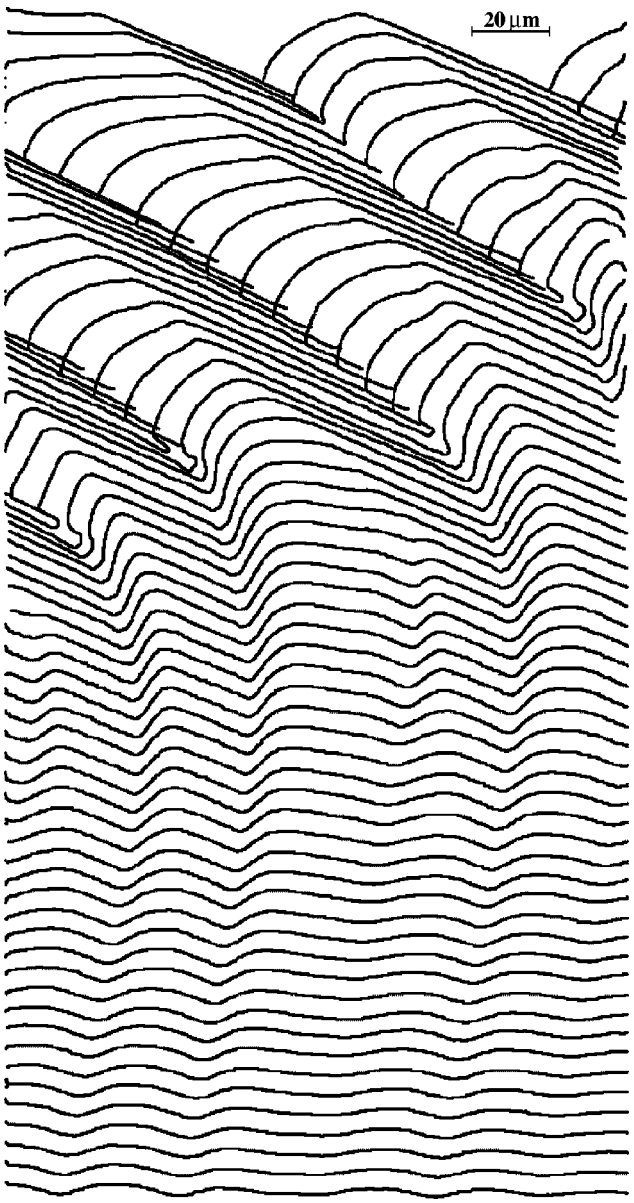

FIG. 17. Facetons appearing in response to a perturbation. Spatiotemporal diagram. $V=6.5\ \mu\mathrm{m\,s^{-1}}$, $\theta_0=25°$, recording time: 60 s. Note the opposite signs of the drift velocities of the cells and the facets.

tainty ($\approx 0.5°$). Thus, the same macroscopic facet may be in two different microscopic states, or growth regimes. One of these (the ''slow'' regime) is that of the stationary state, discussed in the preceding section, while the other (the ''rapid'' regime) corresponds to a rough interface. As announced, we are thus led to assume that the crossover from vicinal to rough interfaces occurs at values of $\delta\theta$ lower than $\approx 0.5°$ in our system. This is indeed surprising since this disorientation corresponds to a very low density of steps (less than 1 per μm), but not impossible. We also note that the persistence of a macroscopic facet while the interface is rough on a microscopic scale is explainable by the sole singularity of the γ plot [16].

The existence of two different growth regimes of a macroscopic facet is confirmed by the fact that facetons most often adopt an oscillatory mode of propagation (Fig. 18). Obviously, this oscillation consists of a more or less ample cycle between the aforementioned rapid and slow regimes. The conditions under which facetons are stationary, or oscillatory, could not be determined. In fact, stationary facetons were observed much less frequently than, and always in coexistence with oscillating facetons. Moreover, some oscillating facetons were regular (Fig. 18), but most of them were irregular (Figs. 13 or 19). It is possible that the system intrinsically admits stationary, periodic, and more or less, chaotic facetons. However, the following explanation is also possible.

A careful inspection of Fig. 18 reveals that the transition of the oscillating facetons from a slow to a rapid regime corresponds to a sudden pinching off of the liquid groove, whereas the reverse transition from a rapid to a slow regime consists of a progressive deepening of the groove. If we focus on the sole groove, this behavior is strongly reminiscent of the periodic pinching off (called cusp instability) of the intercell grooves in nonfaceted cellular fronts [30]. This in-

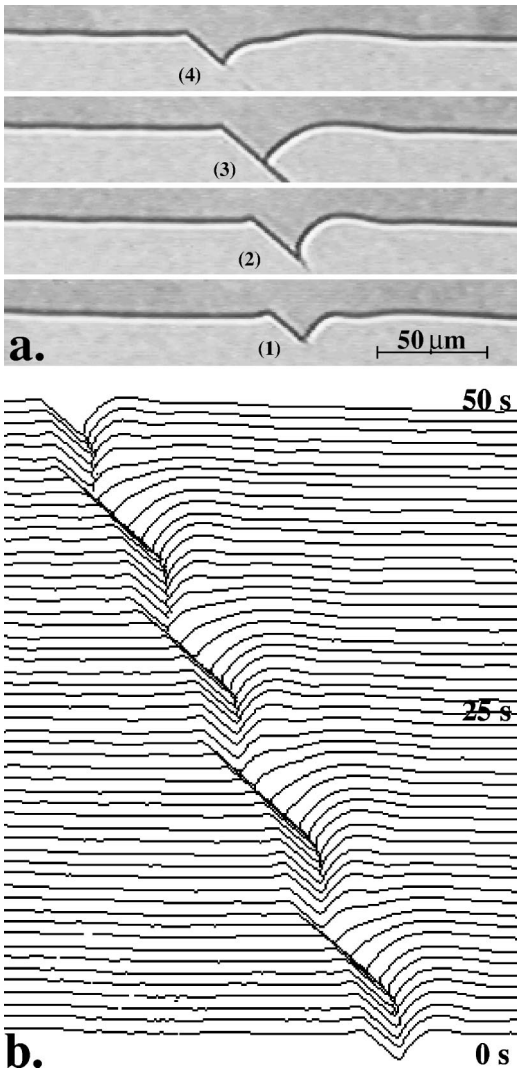

FIG. 18. Oscillating faceton. $\theta_0=42°$, $V=6.5\ \mu\mathrm{m\,s^{-1}}$. (a) Snapshots of the front at different stages of an oscillation period. (b) Spatiotemporal diagram.

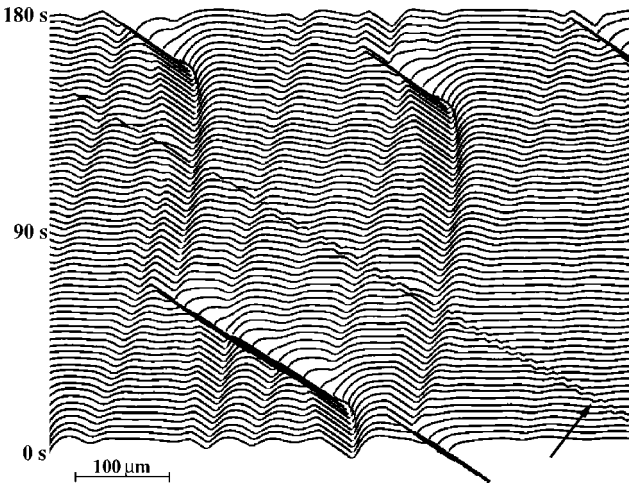

FIG. 19. Spatiotemporal diagram showing shallow cells, oscillating faceted solitary waves, and microfacets (arrow), $\theta_0 = 36°$, $V = 3.1\ \mu\mathrm{m\,s^{-1}}$, and $G = 25\ \mathrm{K\,cm^{-1}}$.

stability, we recall, is most probably of a capillary origin (Rayleigh instability) [31], and very sensitive to the lattice defects that, in the nonfaceted systems, are often attached to the groove—in fact, the grooves to which subboundaries (low-angle grain boundaries) are attached are not subject to the cusp instability [32]. If, by analogy, we assume that the intercell groove of facetons, similar to that of nonfaceted cells, is intrinsically subject to an oscillatory Rayleigh instability, we are led to the conclusion that the transition of the facet from a slow to a rapid regime is a secondary effect due to changes occurring in the configuration of the interface near the lower edge of the facet. The presence of lattice defects (e.g., sub-boundaries) emerging into the liquid at the bottom of the groove may hinder these changes, suppressing the oscillation. This would explain that facetons are much more often oscillatory than stationary.

4. Lattice defects

Some lattice defects (mostly, grain boundaries) may be detected with the optical microscope thanks to the fact that they create macroscopic depressions (grooves) of the growth front around the point at which they emerge into the liquid. In our system, these grooves must be partly faceted during solidification. We have lowered the applied thermal gradient in some experiments in order to facilitate the observation of such grooves. This allowed us to reveal that the growth front of our system is often swept by very small facets, called microfacets, certainly attached to lattice defects emerging into the liquid.

We observed several types of microfacets, corresponding probably to different types of lattice defects. The microfacets of the type shown in Fig. 19 were relatively easy to identify because they travel at a perfectly constant velocity, catching up, and running through all the other structures of the front, in particular, facetons. Their drift velocity has thus most probably the maximum possible value, i.e., the value corresponding to totally blocked facets. They must be attached to lattice defects—stacking faults, or twist subboundaries—strongly locked onto the lamella plane of the smectic. However, these microfacets seem to have but little effect on the dynamics of the front. They indeed provoke an instantaneous slowing down of the macroscopic ''rapid'' facets when they collide with them (see Fig. 19), but do not trigger a durable transition to the slow regime. So this observation, whatever its intrinsic interest may be, does not cast light on the question of the possible role played by lattice defects in the dynamics of the facetons.

V. DISCUSSION

We have shown that the directional solidification of a nematic–smectic-*B* front in the planar configuration gives rise to a wealth of interesting nonlinear phenomena, the most striking of which are the stationary or oscillatory ''facetons'' encountered in the vicinity of the Mullins-Sekerka threshold. These observations raise numerous unsolved problems concerning the microscopic growth mechanisms of the facets, as well as the nonlinear dynamics of the observed macroscopic patterns. An important question is whether these phenomena are specific of the nematic–smectic-*B* fronts, or are of frequent occurrence in partly faceted fronts. In order to clarify this point, we are currently searching for similar phenomena in more conventional, partly faceted solidification fronts. Also, numerical simulations based on a phase-field method are in progress in order to test the consistency of the numerous conjectures that we have been led to make in order to explain the peculiar dynamical features of the facetons.

ACKNOWLEDGMENTS

The authors wish to thank A-M. Levelut for the help in characterizing CCH4 with x-ray diffraction, T. Tóth-Katona and Á. Buka for many useful discussions, and A. Fleury and C. Picard for their technical assistance. We are also grateful to MERCK (Darmstadt) for kindly providing us with CCH4. T.B. would like to thank the European Commission for financial support.

[1] *Solids Far from Equilibrium*, edited by C. Godrèche (Cambridge University Press, Cambridge, England, 1992).
[2] M. Cross and P. Hohenberg, Rev. Mod. Phys. **65**, 851 (1993).
[3] J. Langer. Rev. Mod. Phys. **52**, 1 (1980).
[4] S.R. Coriell and R.F. Sekerka, J. Cryst. Growth **34**, 157 (1976).
[5] P. Kopczynski, W.-J. Rappel, and A. Karma, Phys. Rev. Lett. **77**, 3387 (1996).
[6] F. Melo and P. Oswald, Phys. Rev. Lett. **64**, 1381 (1990).
[7] S. Akamatsu, G. Faivre, and T. Ihle, Phys. Rev. E **51**, 4751 (1995).

[8] S. Akamatsu and G. Faivre, Phys. Rev. E **58**, 3302 (1998).
[9] D.K. Shangguan and J.D. Hunt, Metall. Trans. A **22A**, 941 (1991).
[10] L.M. Fabietti and R. Trivedi, J. Cryst. Growth **182**, 185 (1997).
[11] P. Oswald, F. Melo, and C. Germain, J. Phys. (France) **50**, 3527 (1989).
[12] F. Melo and P. Oswald, J. Phys. II **1**, 353 (1991).
[13] W.K. Burton, N. Cabrera, and F.C. Frank, Philos. Trans. R. Soc. London **243**, 299 (1951).
[14] Á. Buka, T. Tóth-Katona, and L. Kramer, Phys. Rev. E **51**, 571 (1995).
[15] T. Tóth-Katona, T. Börzsönyi, Z. Váradi, J. Szabon, Á. Buka, R. González-Cinca, L. Ramirez-Piscina, J. Casademunt, and A. Hernández-Machado, Phys. Rev. E **54**, 1574 (1996).
[16] R. González-Cinca, L. Ramirez-Piscina, J. Casademunt, A. Hernández-Machado, T. Tóth-Katona, T. Börzsönyi, and Á. Buka, Physica D **99**, 359 (1996).
[17] A.A. Chernov, Contemp. Phys. **30**, 251 (1989).
[18] T. Tóth-Katona, N. Éber, and Á. Buka, Mol. Cryst. Liq. Cryst. Sci. Technol., Sect. A **328**, 467 (1999).
[19] A.M. Levelut (unpublished).
[20] R. Brownsey and A. Leadbetter, J. Phys. (France) Lett. **42**, 135 (1981).
[21] P. Damman, M. Dosière, M. Brunel, and J.C. Wittmann, J. Am. Chem. Soc. **119**, 4633 (1997).
[22] T. Börzsönyi, T. Tóth-Katona, Á. Buka, and L. Gránásy, Phys. Rev. E **62**, 7817 (2000).
[23] J.C. La Combe, M.B. Koss, L.A. Tennenhouse, E.A. Winsa, and M.E. Glicksman, J. Cryst. Growth **194**, 143 (1998).
[24] C. Herring, Phys. Rev. **82**, 87 (1951).
[25] D.R. Ulhmann, in *Advances in Nucleation and Crystallization in Glasses* (American Ceramic Society, Columbus, OH, 1971).
[26] D.R. Ulhmann, in *Nucleation and Crystallization in Glasses* (American Ceramic Society, Columbus, OH, 1982).
[27] T. Börzsönyi, S. Akamatsu, and G. Faivre (unpublished).
[28] J.A. Warren and J.S. Langer, Phys. Rev. E **47**, 2702 (1993).
[29] A.A. Chernov, S.R. Coriell, and B.T. Murray, J. Cryst. Growth **132**, 405 (1993).
[30] P. Kurowski, S. de Cheveigné, G. Faivre, and C. Guthmann, J. Phys. (France) **50**, 3007 (1989).
[31] K. Brattkus, J. Phys. (France) **50**, 2999 (1989).
[32] S. Bottin-Rousseau, S. Akamatsu, and G. Faivre (unpublished).